Spatial and temporal variation of water reflectance in an Amazonian estuary: a case study around Tatuoca Island

Matheus Dias de Aviz [1], Jean-Michel Martinez [2,3], Laurent Polidori [1]

[1] Post Graduate Program in Geology and Geochemistry, Institute of Geoscience, Federal University of Pará (UFPA), Brazil - matheus.aviz@ig.ufpa.br, laurent.polidori@ird.fr

[2] Institute of Geosciences, University of Brasília (UNB), Brazil - jean-michel.martinez@ird.fr

[3] UMR GET IRD/CNRS/UPS, Toulouse, France- jean-michel.martinez@ird.fr

Keywords: Semivariance, ANOVA, Pará River, Suspended Sediment, Sampling.

Abstract

Studies of water color are related to its optically active components, including suspended sediments. The correlation of this parameter with reflectance data is well documented in the literature, to understand its concentrations and transport in the water body. The spatio-temporal variations of water color in an estuary are affected by various physical and hydrological components, which makes it complex to understand. In this study, we sought to understand the spatio-temporal variation of water color, for sampling purposes, in an estuary on the Amazon coast. To achieve our objectives, we applied geostatistical and statistical tools to test the spatio-temporal variability of water color, based on multisensor reflectance data, Landsat-8/9 and Sentinel-2 in the red band. The spatial variation showed distances of more than 48 m ±4.26 at high tide and 44 m ±7.62 at low tide. For the temporal variation, we found that the monthly variations are significant according to seasonality and have the same variation at different stages of the tide. Therefore, the color of the water in the Tatuoca Island region shows geostatistically and statistically significant spatio-temporal variation. The distances and temporal frequency of sampling should be adjusted according to the tides and seasonality to ensure that data is sampled in accordance with the variations in the environment.

1. Introduction

The optical properties of water are related to its composition, enabling research and monitoring of aquatic ecosystems. Remote sensing of water color is an area of study that makes it possible to extract information from aquatic environments with wide spatial and temporal coverage (Zhang et al., 2017). Research on water color is related to measurement and modeling studies of bio-optical properties (Guillaume et al., 2023), atmospheric correction and data uncertainties (Zhang et al., 2022), remote sensing algorithms for chlorophyll-a and suspended sediments (Kupssinskü et al., 2020), chromophoric dissolved organic matter (CDOM) (Qiang et al., 2023), and water quality and water ecology (Pan et al., 2022).

The majority of studies on water color have employed field collections to validate or calibrate the results. Studies on water color in the Amazon have utilized high- to medium-resolution sensors. Some studies have already indicated that high- to moderate-resolution satellite data could be an alternative to achieve more accurate results (Fassoni-Andrade and Paiva, 2019). However, the effect of the lag between field and satellite overflights remains unclear. Most studies assume that field and orbital data were collected at the same time. Consequently, the impact of spatial and temporal discrepancies between collection and overflight remains under-researched (Gao et al., 2023).

To understand water color, analyze optical agents and environmental variables, especially in estuaries, where complexities such as tides, waves, currents, river flows, sediment transport, erosion, accretion, wind, and climatic influences impact hydrodynamics (Azevedo et al., 2023).

The article aims to analyze how sedimentation varies over space and time in water, to develop appropriate sampling methods for the local conditions. It suggests that changes in water color significantly affect where samples should be taken due to the area's complexity. This region is an estuarine zone affected by tides, containing high sediment levels and diverse landforms. Monitoring water color variations is crucial for calibrating and correlating reflectance with water composition. Thus, it's vital to align sampling points with spatial and temporal variations during water sampling.

The study aimed to investigate how water color varies over space and time in an estuary on the Amazon coast, an area lacking observation stations in the hydrological observatory network. We employed geostatistical and statistical methods to understand this variation. Our goal was to establish the spatial and temporal boundaries for sampling sites, guiding the selection of collection stations aligned with these variations. This will enhance calibration and correlation with orbital data, considering seasonal and tidal influences in the Tatuoca Island region.

This paper will examine the techniques employed to ascertain variations, utilizing geostatistical tools for spatial variation and statistical tools for temporal variation. It will present metrics and indicators derived from the respective techniques and demonstrate how they inform the determination of the variations under investigation.

This contribution has been peer-reviewed. The double-blind peer-review was conducted on the basis of the full paper.
https://doi.org/10.5194/isprs-annals-X-3-2024-29-2024 | © Author(s) 2024. CC BY 4.0 License.

2. Methods and Materials

2.1 Area of study

The study area is located in the estuary formed by the confluence of the Pará (Tocantins and 5% of the Amazon), Guamá and Acará rivers, downstream from the city of Belém, near the island of Tatuoca (Figure 1). This island is located between two important bays, Marajó and Santo Antônio, which in turn have different bottom morphologies that influence the region's currents.

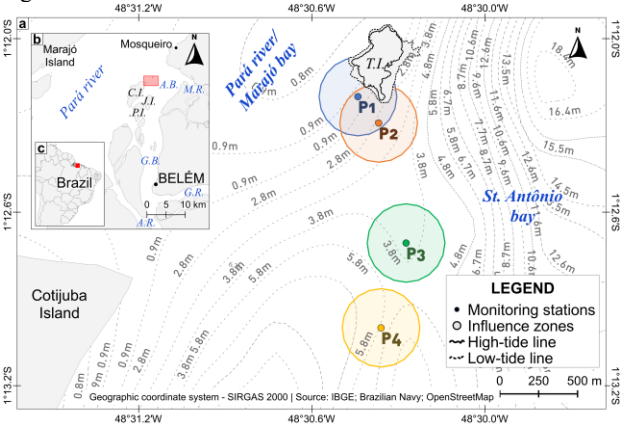

Figure 1. Location of the study area. a: Tatuoca region; b: Location in Belém; c: Location in Brazil; A.B.: Santo Antônio Bay; G.B.: Guajará Bay; C.I.: Cotijuba Island; J.I.: Jutuba Island; P.I.: Paquetá-Açu Island; T.I.: Tatuoca Island; A.R.: Acará River; G.R.: Guamá River; M.R.: Maguari River.

In this region, there are two seasons, the rainy season (December to May) and the less rainy season (June to November). Despite being 50 km away from the coast, tides still impact the area. The tidal patterns observed in the estuary can be classified as meso- and macro-semidiurnal tides, with an average tidal range of 3.2 m. The average difference between high and low tides ranges from 0.5 m to 1.2 m, with a minimum low tide height of about 2 m (Preste et al., 2017).

The island is about 5 ha in size and situated 10 km from Belém's mainland, positioned between a 15-metres-deep channel on the right side and shallow areas averaging 4 m in depth on the left. Located in the estuary mixing zone of the Pará River, it experiences intricate interactions between river flow and tides, shaping distinct environmental conditions crucial for sediment dynamics and biogeochemical processes.

Tatuoca Island, managed by the Brazilian National Observatory, houses a permanent team for geomagnetic monitoring. Though closed to the public, it offers convenient access (30 minutes by boat), solar energy, internet access, and office. With these features, it is well-suited for inclusion in the hydrological observatory network, providing a station in an estuarine environment.

2.2 Image acquisition

For the spatial analysis, we used Sentinel-2 images, level 2A, available on the Google Earth Engine - GEE platform, in the collection (COPERNICUS/S2_SR_HARMONIZED), already corrected for the atmosphere. In the spatial analysis, the months of June, July, and August 2023 were studied due to the lower cloud cover. We selected high and low tide images under the same conditions, i.e. we considered the height and state of the tide (rising or falling) whenever possible. For the temporal analysis, we used collections of Landsat-8 and 9, level 2 and Sentinel-2, level 2A images available on the GEE platform in the collections (LANDSAT/LC08/C02/T1_L2, LANDSAT/LC09/ C02/T1_L2 and COPERNICUS/S2_SR_HARMONIZED, COPERNICUS/S2_HARMONIZED), these with atmospheric correction, except for 'COPERNICUS/S2_HARMONIZED'. The analyzed years were 2014 to 2023.

All sensors utilized the red band (636-673 nm) due to its sensitivity to inorganic components of water. The spatial resolutions differed, with Landsat images at 30 m and Sentinel images at 10 m. The platforms of these sensors passed over the region at similar times around ~10:30 (UTC -3). New images were captured every 15 days by Landsat-8 and 9 and every 5 days by the Sentinel-2 constellation.

Level 2A processing of Sentinel-2 images and Level 2 processing of Landsat-8 and 9 images include geometric corrections to eliminate spatial distortions and radiometric corrections to standardize pixel intensities. This enhances data accuracy for diverse monitoring applications. Sentinel-2 Level 1C images only feature geometric corrections, necessitating corrections using the Sen2Cor algorithm in the SNAP software (SNAP, Development Team, 2022).

2.3 Environmental data acquisition

We obtained precipitation data from the National Meteorological Institute of Brazil (INMET) for the period 2014 to 2023 from the conventional station in Belém (82191), comprising daily and monthly total precipitation in mm. Additionally, we obtained 30 years of rainfall data from the same station to establish a historical average. Tidal data in meters were acquired from the Brazilian Navy at the Ilha do Mosqueiro station (10525) for the same period, extracted only on the dates corresponding to the satellite images used. Finally, discharge data in m^3/s were acquired from the Brazilian National Water Agency (ANA) for Marabá-PA (29050000) on the Tocantins River and Óbidos-PA (17050001) on the Amazon River.

2.4 Image processing and reflectance data acquisition

For spatial analysis, we established a 250 m influence area around the monitoring points. Within these areas, each pixel of the images was converted into vector points. Processing was conducted in GEE, where we implemented masks to eliminate pixels containing clouds, shadows, and cirrus effects. Reflectance values in the red band were then extracted for each vector point. Temporal analysis was also performed in GEE. Images were corrected as needed to remove atmospheric interference, and masks were applied to eliminate pixels with clouds, shadows, and cirrus effects. Reflectance values in the red band were extracted for the four monitoring points.

2.5 Geostatistics and statistics

The analyses were conducted using reflectance values to eliminate possible atmospheric interference and to standardize the results to ensure consistency between different sensors and different dates. The process of standardizing image data in reflectance is intended to ensure consistency and comparability between different data sets in a multi-sensor, multi-data approach. To ensure the integrity and reliability of the results, we proceeded to remove outliers using the interquartile limits

method. The purpose of this step is to eliminate discrepant values that could bias the analysis and subsequent interpretations. The presence of outliers in data used in parametric analyses can have several undesirable effects, such as increasing meaningless variability.

2.5.1 Geostatistics: Reflectance data spanning three months were obtained through image processing on the GEE platform. These data were subsequently imported into PASSaGE® (Rosenberg and Anderson, 2011) for geostatistical analysis, with analysis distances tailored to image resolution.

Following preprocessing and initial definitions, spatial variance, normality, Moran's I coefficient, anisotropy determination, and stationarity were assessed before constructing the semivariogram.

Spatial variance evaluates data variability across spatial locations, revealing heterogeneity patterns and spatial autocorrelation. Normality checks ensure the validity of parametric tests. Moran's I coefficient evaluates spatial autocorrelation, indicating correlations between neighboring locations. Anisotropy determination examines spatial correlation directionality. Stationarity tests consistency of statistical properties across spatial locations, ensuring analysis validity. These analyses are crucial for understanding spatial patterns and processes in the data.

After identifying patterns, semivariograms were plotted using ArcGIS® software and cross-validated to analyze model errors. Validated semivariograms aid in identifying spatial variability, facilitating the determination of trends, patterns, or anomalies.

2.5.2 Statistics: Reflectance data collected over a 10-year period from study points underwent image processing on the GEE platform and statistical analysis in r Studio.

Following data preprocessing, one-way analysis of variance (ANOVA) and Tukey-Kramer post-processing were conducted to identify temporal variation and groupings. ANOVA assessed significant differences between data groups across different time periods, while the Tukey-Kramer test enabled multiple comparisons to identify statistically significant differences between these periods. These analyses provided insights into seasonal patterns and trends over time.

Additionally, analyses of normality, ANOVA, and significance were performed, comparing reflectance data with monthly precipitation, flow and tide data. The analysis significance indices were plotted to identify trends, patterns, or anomalies across years and environmental variables such as seasonality and tide.

3. Results

3.1 Spatial analysis

To assess the spatial variation of reflectance in the Tatuoca region, we applied geostatistics to the reflectance data from the satellite images, using the field collection points as a geographical reference. Our analysis revealed that the reflectance data exhibited spatial variations in different directions, ranges, and distances. These variations exhibited distinct responses to the tide, with high and low tides influencing the reflectance data in different ways. The spatial analysis was confined to an examination of the less rainy period.

3.1.1 Autocorrelation: The spatial variation of directions, ranges, and distances was determined using geostatistics. Initially, the spatial dependence of the data was determined using Moran's I correlograms, which indicate whether nearby individuals correlate (Moran, 1950).

The Moran's I coefficient values are significantly close to +1 at short distances at high tide. This indicates that the reflectance values exhibit the following Moran's correlation coefficients: at 25 m, 0.75 ±0.14; at 50 m, 0.56 ±0.14. At low tide, the correlation coefficients were 0.55 ±0.20 at 25 m and 0.43 ±0.19 at 50 m. Points 1 and 2 exhibited the highest correlation coefficients at both states of the tide. Points 3 and 4 exhibited the lowest correlation coefficients. This suggests that at short distances (>50 m), we can correlate the data and apply spatial variation models to assume distances of variation in water color. It is therefore proposed that samples geographically closest to the field collection points exhibit greater similarity in reflectance values, while those geographically distant exhibits greater dissimilarity. Furthermore, it is postulated that the tide exerts a significant influence on the similarity coefficient.

3.1.2 Anisotropy: Correlograms are omnidirectional but can exhibit variation in spatial autocorrelation across specific directions. Anisotropy was assessed using Simon's angular correlation method, analyzing the degree of anisotropy in two-dimensional data.

Figure 2 displays angular correlograms, with geographic north represented by the 90° angle. Circular shapes in angular correlograms indicate preferred correlation directions, reflecting temporal variations such as tide and month. It is important to note that the tides in this region exhibit semi-diurnal cycles with a period of approximately six hours per cycle.

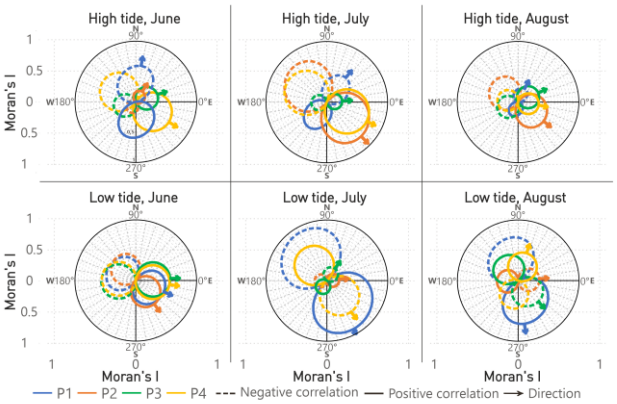

Figure 2. Angular correlograms

The elliptical shapes signify anisotropy, where spatial autocorrelation varies across directions, implying geometric anisotropy with fluctuating correlation ranges but consistent patterns formed by tidal currents during high tide.

Observations during high tide predominantly showed a SW-NE trend, except for point 2 in June, displaying both SW-NE and NW-SE trends. Conversely, during low tide, point 1 consistently displayed a NW-SE direction across all months, while other points lacked clear directional preferences, reflecting the complex interplay of seasonal and localized factors in estuarine dynamics.

Point 3 consistently exhibited low correlation intensity across all months and tidal states, indicating heterogeneous sediment distribution. Local sediment sources may dominate at short distances, while a mixture of sediments from varied origins at greater distances results in weaker correlation due to differing optical properties.

3.1.3 Semivariance: A Based on the findings of spatial autocorrelation and the ideal distance and preferred direction, we defined benchmarks to test the variance of the reflectance data. For this test, we employed semivariograms, the principal form of spatial analysis utilized in geostatistics. The distances of the Moran's I correlogram and the angles of directions of the angular correlogram were utilized in the semivariogram model (Figure 3).

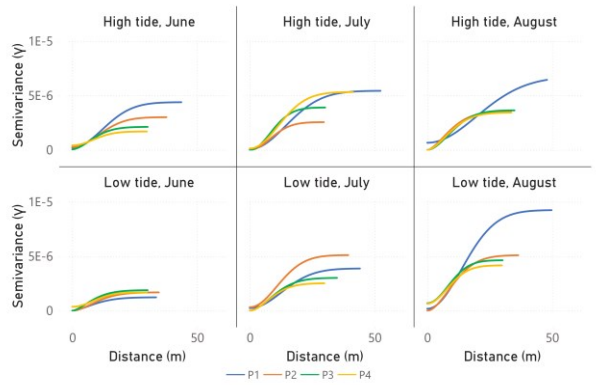

Figure 3. Anisotropic semivariograms

Semivariograms illustrated varying distances (m) and semivariance (γ) between points and tidal states, with angular correlograms depicting directions. Semivariance range and maximum distance with the least spatial variance were represented, quantifying data variability concerning distance (lag) with a low nugget effect, suggesting adequate model use (Simon, 1997).

Different patterns emerged during high and low tides, with high tide showing more consistent semivariance values among points, indicating homogeneous spatial sediment distribution (3.59^{-6} ±1.41^{-6} at high tide, 3.45^{-6} ±2.24^{-6} at low tide). Point 1 consistently exhibited the highest semivariance values in monthly comparisons. However, at low tide, variability increased over time while maintaining similar semivariance.

The distance between points varied between high and low tides (median distances: 48 m ±4.26 at high tide, 44 m ±7.62 at low tide), with Point 1 consistently showing high distance values at both. Generally, distances were more consistent at low tide, suggesting a more homogeneous spatial distribution, while high tide exhibited a more heterogeneous distribution. Nonetheless, the slight difference between distributions can be attributed to the nugget effect, indicating that observed values are modeled estimates.

3.2 Temporal analyses

Statistical analysis of reflectance data in the Tatuoca region, using spatial analysis points as reference, revealed temporal patterns throughout the year. Reflectance peaks were noted in central zones of seasonal periods, with decreases in transition zones. Environmental forcings like tides and seasonality were assessed using variables including rainfall, tide level, and categorical distinctions between rainy and less rainy seasons, and high and low tides based on regional averages. This analysis covers all seasonal periods, but there is a greater amount of data from the less rainy period.

Median reflectance during the rainy season (0.0730 ±17.72^{-3}) was lower than in the less rainy season (0.0885 ±23.12^{-3}), despite fewer cloud-free images during the rainy period. However, reflectance values during the less rainy period didn't significantly surpass those in the rainy period, with similar peak levels observed in both.

Reflectance behavior varied with tidal conditions. In the rainy season, high tide showed peaks in January (0.0955 ±8.77^{-3}) and March (0.0960 ±17.25^{-3}), decreasing in May (0.0580 ±17.55^{-3}). Conversely, during the less rainy season, peaks occurred in October (0.1120 ±22.07^{-3}) and November (0.1055 ±26.33^{-3}), decreasing in June (0.0585 ±9.42^{-3}). At low tide, peaks were observed in February (0.1075 ± 9.58^{-3}) and October (0.0975 ± 23.19^{-3}) during the rainy and less rainy seasons respectively, with decreases in May and June.

Data analysis revealed that high tide exhibited higher peak values and lower base values than low tide in both seasonal periods, while low tide exhibited lower peak values and higher base values than high tide. These observations underscore the significant influence of seasonal cycles on water reflectance.

3.2.1 The reflectance behavior related to environmental variables: Reflectance levels follow a cyclical pattern throughout the year, peaking during seasonal periods and tidal intervals, with lower levels in the first semester and higher levels in the second.

Correlation between downstream river flow levels and reflectance is evident, supported by data from ANA stations. For example, peak flows at Marabá station on the Tocantins River reached 31,000 m³/s, while at Óbidos station on the Amazon River, peak flows were 273,000 m³/s (ANA, 2022). Reflectance shows a stronger correlation with low tide data, indicating greater fluvial influence.

Seasonal changes affect sediment transport, impacting reflectance levels year-round. Precipitation locally shows no direct correlation with reflectance but indirectly affects flow and reflectance through downstream river basin precipitation.

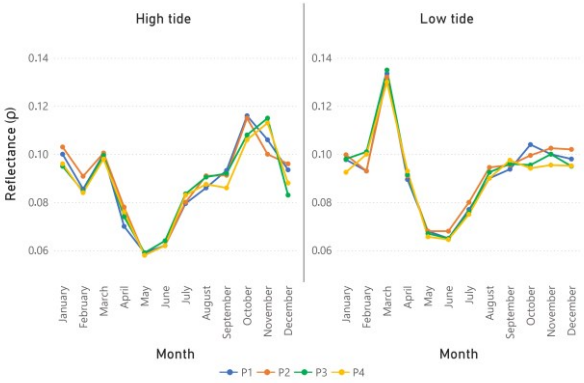

Figure 4. Median reflectance per month at different tides

Figure 4 displays median graphs illustrating reflectance levels during high and low tides, revealing fluctuations attributed to seasonal and flow changes. Reflectance medians at high tide

This contribution has been peer-reviewed. The double-blind peer-review was conducted on the basis of the full paper.
https://doi.org/10.5194/isprs-annals-X-3-2024-29-2024 | © Author(s) 2024. CC BY 4.0 License.

(0.0845 ±22.60^{-3}) and low tide (0.0830 ±22.22^{-3}) exhibit significant variation throughout the year due to seasonal changes, river flows, and tide level fluctuations. Peaks in May and October, along with minimum values in May and June, are evident across both tidal states. The tides undergo a change approximately every six hours, exhibiting distinct states that can contribute to the observed variation in reflectance. This phenomenon can be employed to inform broader interpretations.

In response to observed reflectance variations, we conducted an analysis of variance (ANOVA) to assess variability across the 12 months of the year, with results detailed in Table 1.

Point	Sum Sq	Mean Sq	F value	Pr(>F)
P1	0.05074	0.004612	18.93	<2^{-16} *
P2	0.04938	0.004489	18.32	<2^{-16} *
P3	0.05100	0.004636	20.09	<2^{-16} *
P4	0.04970	0.004518	19.27	<2^{-16} *

Table 1. ANOVA summary.

The statistical analysis, including Sum Sq, Mean Sq, F value, and Pr(>F) with "*" indicating high significance ($p < 0.001$), revealed significant differences between months, indicating substantial temporal variability influenced by tides and seasonality.

Upon identifying these disparities, a Tukey-Kramer test was applied to group statistically similar months. Across all ANOVAs, the "month" factor significantly impacted point values ($p < 0.05$), signifying significant monthly differences. Months were grouped into six categories (a-f), he Tukey-Kramer test grouped months as follows: Group a: Feb, Mar, Sep, Oct, Nov, and Dec; Group b: Jan, Feb, Mar, Aug, Sep, Nov, and Dec; Group c: Jan, Feb, Mar, Apr, Aug, Sep, and Dec; Group d: Jan, Apr, Jul, and Aug; Group e: Apr, May, and Jul; Group f: May and Jul, each sharing similar reflectance characteristics determined by statistical analysis.

For instance, January months consistently showed no statistical difference in reflectance across years, reinforcing the reliability of temporal variation analyses and interpretations.

3.2.2 The behavior of reflectance over a period of ten years: The analysis of reflectance over the ten-year period shows fluctuations, with increases and decreases observed from year to year. Notable inter-annual variations are evident, with some years showing more pronounced patterns of change compared to others. River flow and tides are clearly significant factors influencing reflectance, as depicted in Figure 5.

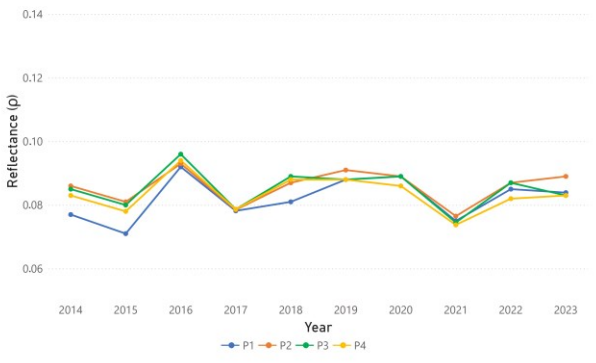

Figure 5. Median reflectance per year.

Between 2014 and 2023 (Figure 5), Point 1 exhibited the greatest increase (8.96%), while Point 3 exhibited the greatest decrease (2.35%). Across all metrics, point 4 exhibited the most intriguing recent trend, initiating a decline in 2019, resulting in a 5.68% decrease over a four-year period. Point 4 experienced a significant decline, falling from ~0.090 to ~0.080, during the most pronounced decline between 2019 and 2023.

Additionally, the study observed occasional one-off events, such as years with recorded peaks or higher reflectance, alongside periods of more stable conditions. Despite inter-annual fluctuations, there were stretches when reflectance showed relatively consistent behavior over several months.

However, over the ten-year study period, reflectance exhibited significant variability. While some years experienced isolated increases in reflectance, no consistent long-term trend emerged. The presence of clouds, especially during the first half of the year, might have affected the accuracy of data collection.

4. Discussion

The study aimed to explore spatio-temporal water color variation in the Tatuoca Island region, considering seasonality and tide effects. Analysis unveiled distinct patterns, with varying sampling distances during different tide levels and consistent seasonal uniformity across study years. These findings offer valuable insights into local water color dynamics, informing sampling and monitoring strategies.

Spatial analysis revealed differences in sampling distances, with median of 48 m ±4.26 at high tide and 44 m ±7.62 at low tide, reflecting tidal dynamics' influence on water color behavior. Similar spatial sampling distances of 31 m at high tide and 27 m at low tide were inferred.

Temporal analysis showcased monthly variations in water color uniformity over a decade, indicating a consistent pattern across months. However, daily variation was not captured due to image temporal resolution (minimum of 5 days). Temporal sampling determination was inferred to be similar across months, given the low variation observed over the analyzed series.

4.1 Spatial variation

Tide emerged as the primary driver of spatial water color variation, supported by strong correlations and semivariance results at high tide compared to low tide. The region's consistent hydrodynamics, influenced by bottom morphology, river input, and tidal regime, contribute to observed spatial patterns. Previous studies by Silva et al. (2020) corroborate these findings, highlighting the role of tidal influence in altering water turbidity and sediment distribution.

4.1.1 The alterations in river discharge: During the less rainy period, characterized by lower river discharge compared to the wettest period, estuary discharge was approximately 13,000 m³/s, significantly lower than the wettest period's average of around 28,000 m³/s (Prestes et al., 2020).

This reduction in river discharge notably impacts sediment transportation and dispersion within the Pará river estuary, allowing the salt wedge to penetrate deeper, altering water color depending on the tide phase.

This contribution has been peer-reviewed. The double-blind peer-review was conducted on the basis of the full paper.
https://doi.org/10.5194/isprs-annals-X-3-2024-29-2024 | © Author(s) 2024. CC BY 4.0 License.

The Pará River's water input shifts from sediment-rich rivers like the Amazon and Guamá to the Tocantins River, which has lower sediment content. Prestes et al. (2020) found that the Araguaia-Tocantins River basin contributes 52% of the discharge to the Pará River, with the Amazon basin contributing 44%. Seasonal variations show the Tocantins River contributing more to the first half of the year, while the Amazon Basin contributes more in the second half. Despite reduced river discharge, sediment transportation remains substantial during low tide due to strong water discharge continuing to push seawater, resulting in increased turbidity and sediment dispersion on the surface (Gensac et al., 2016).

4.1.2 Tidal dynamics and their impact on water color: During high tide, the Pará River estuary witnesses a substantial seawater influx annually, ranking fifth globally at 664 km³ (Prestes et al., 2020). Conversely, low tide sees significant river water and sediment flow seaward, altering estuarine volume, current direction (NE), and water color. River dominance during low tide slows currents, impacting sediment transport (Azevedo et al., 2023).

These effects manifest in volume, current direction (southwest), and water color. Higher water volume alters currents, resulting in distinct color zones influenced by river currents and oceanic forces. Slower currents during low tide increase sediment settling but lead to more uniform water color due to fine sediment dispersion.

In low-energy tidal current areas, less turbid zones are within channels, while turbid zones form due to underwater relief and tidal currents (Figure 6). Minimal mixing allows clear spatial distinctions (Azevedo et al., 2023). Turbid zones in shallow areas contrast with less turbid ones in deeper areas, influenced by weak currents and the region's geological composition (Corrêa, 2005).

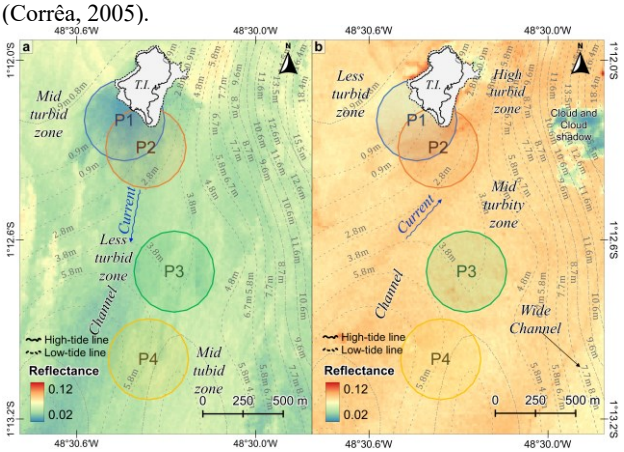

Figure 6. Turbidity zones according to the tide. A: High tide, Sentinel-2 (04/Jul/2023); B: Low tide, Sentinel-2 (09/Jul/2023); T.I.: Tatuoca island. Linear false-color slicing of the red band.

Distinct turbid and less turbid color zones create sharp transitions, influenced by current patterns, impacting reflectance due to varying suspended sediment levels (Zhan et al., 2019).

Even during low tide, turbid zones persist, predominantly distributed across the region. Varied topographies and current velocities contribute to sediment dispersion, with higher relief areas promoting sediment deposition and increased turbidity. Tatuoca Island's damming effect enhances sediment accumulation, resulting in uniform water color and widespread sediment dispersion (Cruz, 2005). Elevated suspended sediments significantly alter reflectance levels within these zones (Toniolo et al., 2018).

4.1.3 Implications of tides on special variation metrics: Spatial analysis highlighted tidal configurations influencing spatial dependence and water color variability across monitoring areas.

High tide exhibited less spatial dependence and greater variability at shorter distances, while low tide showed increased spatial dependence and reduced variability (Amaral et al., 2013). Significant differences in collected data were observed during high tide, with spatial dependence over longer distances and lower variability, while low tide showed smaller differences, attributed to color homogeneity from hydrodynamic interactions (Farzaneh et al., 2022).

Tidal currents significantly influenced sedimentary phenomena, impacting spatial variability metrics and generating distinct results. Seasonality testing is crucial for understanding changes in water color geometric features, potentially affecting correlations and spatial dependence. Distinct color zones formed due to ocean water entry and current redirection by Tatuoca Island, influenced by its presence altering current direction and sediment distribution (Toniolo et al., 2018).

Different water colors stemmed from tidal current velocities influenced by bottom geomorphology, particularly channels and their geometries, which unevenly distributed transported or suspended sediments (Azevedo et al., 2023). Average current speeds supported the formation of distinct turbidity zones due to ocean water influx.

4.2 Temporal variation

4.2.1 Seasonal effects on reflectance: Seasonality emerges as the primary driver of temporal reflectance variation, evidenced by spectral responses aligning with seasonal cycles. Variance tests confirm distinct monthly reflectance groupings, reflecting seasonal patterns. Reflectance variation is influenced by seasonality, impacting water characteristics and estuarine dynamics (Gensac et al., 2016).

Tidal and seasonal cycles jointly influence reflectance. High tide during the rainy season decreases reflectance due to increased water influx and sediment dilution (Zhan et al., 2019). Conversely, high tide in the less rainy period elevates reflectance due to higher sediment concentration. Reflectance peaks during the less rainy period due to reduced water volume (Gensac et al., 2016).

Unexplained variations, possibly linked to climatic events like 2021's low median reflectance, underscore the impact of changing seasonal cycles (Morera et al., 2017). Heavy rainfall, especially in the first half of the year, leads to increased cloud cover, potentially biasing analyses due to smaller rainy season datasets (Fu et al., 2022).

While cloud incidence correlates with regional rainfall, it indirectly impacts reflectance by altering river flow and water color over time. Significant changes in water properties, driven by factors like freshwater discharge and stratification, shape seasonal sediment dynamics (Zhan et al., 2019).

A comprehensive understanding of sediment transport dynamics necessitates sediment modeling across the seasonal cycle,

emphasizing the need to differentiate between seasonal periods for precise statistical outcomes.

4.2.2 Implications of sediments on reflectance: Seasonal changes profoundly impact river volume and flow, altering water color due to shifts in rainfall and subsequent runoff. Variations in water color reflect changes in sediment concentration, affecting reflectance through light scattering.

Fluctuations in water volume contribute to reflectance changes, influenced by tides affecting sediment transport. Reflectance oscillations correlate with sediment concentration fluctuations on lunar and seasonal scales, with increased suspended sediment enhancing reflectance. Reflectance exhibits daily and quarterly variations due to the tidal cycle and seasonality (Gardner et al., 2021).

Understanding temporal variation is complex due to variations in water hue and opacity, influenced by sediment load and tidal dynamics. The lunar cycle significantly impacts sediment concentration, leading to varying reflectance alterations. Tidal dynamics strongly influence sediment concentration, affecting transport and dispersion (Carneiro et al., 2020).

Testing the response at all tide stages in different seasonal periods is proposed to understand variations in sediment concentration and their implications for reflectance.

4.2.3 Implications of climatic phenomena over the decade on reflectance: Reflectance exhibited annual and seasonal variability over the analyzed decade, with overall stability. Minor inter-annual fluctuations were potentially influenced by temperature variations linked to El Niño and La Niña phenomena in the Pacific Ocean (Morera et al., 2017), impacting global atmospheric circulation, moisture transport, and precipitation patterns.

ENSO phenomena influence the relative frequency of precipitation, affecting annual reflectance fluctuations. Increased precipitation rates can elevate river water discharge, enhancing sediment transport capacity (Morera et al., 2017), consequently impacting reflectance values (Toniolo et al., 2018). Long-term water monitoring should account for such climatic phenomena.

Understanding climatic influences on water color, including flow, volume, and temperature patterns, is crucial for interpreting reflectance variations, particularly sediment discharge patterns.

4.2.4 Statistical implications for temporal metrics: ANOVA tests revealed statistically significant differences between months, indicating distinct reflectance distribution across the year. Tukey-Kramer test further confirmed these results, revealing three distinct groups: rainy, less rainy, and transitional periods, supporting interpretations of seasonal reflectance variation.

However, ANOVA equality and order restrictions may introduce heterogeneity in data distribution over time (Fu et al., 2022). It's advisable to employ more robust methods to identify influences of tidal and sediment transport on clusters. Regarding sampling implications, ANOVA results suggest consistency in water color behavior within the same month across the analyzed series. Cloud cover during the rainy season posed challenges in trend identification, complicating analysis and reflectance level determination (Fu et al., 2022). Daily variation trends couldn't be established due to image time scale limitations.

Suggesting a multisensor approach with daily temporal resolution. To address data heterogeneity and temporal variability, robust statistical methods like time series analysis or mixed models are recommended. Furthermore, the utilization of multiple bands, such as the BLUE, GREEN and NIR bands, has been demonstrated to be an effective approach for sediment analysis. The exclusive utilization of the red band constrains the scope of the analysis to the establishment of concentrations and the provision of more precise variation inputs. Nevertheless, an understanding of light variation is essential for more specific applications, such as the estimation of sediment concentration.

5. Conclusion

This study demonstrates that water color in the Tatuoca Island region exhibits significant spatial and temporal variation. It is therefore recommended that the distance and frequency of sampling be adjusted according to tides and seasonality to ensure that data is collected with the effects of variation on it.

The analysis of the spatial autocorrelation of water color in the Tatuoca Island region reveals the influence of tides, underwater relief and hydrodynamics. The implications for data collection are significant and must be considered to guarantee the quality and representativeness of the results.

The analysis of the temporal variation of water color in the Tatuoca Island region reveals the influence of seasonality, global climatic phenomena, and cloud cover. The implications for data collection and long-term monitoring of water color are significant and should be considered to ensure the quality and representativeness of the results.

Finally, it is recommended that robust statistical tools be employed that consider the heterogeneity of the data to better understand the seasonal influence on reflectance. Furthermore, the use of atmospheric corrections is advised for the purpose of studying aquatic optics. The present study analyzed a single spectral band (RED), which may have introduced a bias in the findings regarding spatio-temporal variation. It is recommended that other bands, particularly those in the GREEN, BLUE and NIR ranges, be considered for incorporation into sediment estimation concentration models. Finally, data on a smaller spatio-temporal scale is required to delimit these variations on a shorter scale, which was not possible with the orbital data available.

References

Amaral, L. de P., Ferreira, R.A., Watzlawick, L.F., Longhi, S.J., Sebem, E., 2013. Influência da floresta alterada na distribuição espacial de três espécies da Floresta Ombrófila Mista avaliada pela geoestatística. *Revista Árvore* 37, 491–501. https://doi.org/10.1590/S0100-67622013000300012

ANA, Agência Nacional de Águas, 2022. Dados das séries históricas das estações convencionais da Agência Nacional de Águas e Saneamento Básico. github.com/anagovbr/hidro-dados-estacoes-convencionais (accessed 10.20.23).

Asp, N.E., Gomes, V.J.C., Schettini, C.A.F., Souza-Filho, P.W.M., Siegle, E., Ogston, A.S., Nittrouer, C.A., Silva, J.N.S., Nascimento, W.R., Souza, S.R., Pereira, L.C.C., Queiroz, M.C., 2018. Sediment dynamics of a tropical tide-dominated estuary:

Turbidity maximum, mangroves and the role of the Amazon River sediment load. *Estuary Coast Shelf Sci.* 214, 10–24. https://doi.org/10.1016/J.ECSS.2018.09.004

Azevedo, T.N.A., El-Robrini, M., Saavedra, O.R., 2023. Assessment of tidal current potential in the Pará River Estuary (Amazon Region – Brazil). *Cleaner Energy Systems* 6, 100091. https://doi.org/10.1016/J.CLES.2023.100091

Carneiro, A.G., Prestes, Y.O., Rollnic, M., 2020. Estimates of suspended solid transport in the Pará River Estuary. *Ocean and Coastal Research* 68, e20281. https://doi.org/10.1590/S2675-28242020068281

Corrêa, I.C.S., 2005. Aplicação do Diagrama de Pejrup na Interpretação da Sedimentação e da Dinâmica do Estuário da Baía de Marajó-PA. *Pesquisas em Geociências* 32, 109–118. https://doi.org/10.22456/1807-9806.19551

Cheng, Z., Jalon-Rójas, I., Wang, X.H., Liu, Y., 2020. Impacts of land reclamation on sediment transport and sedimentary environment in a macro-tidal estuary. *Estuary Coast Shelf Sci.* 242, 106861. https://doi.org/10.1016/J.ECSS.2020.106861

Farzaneh, G., Khorasani, N., Ghodousi, J., Panahi, M., 2022. Application of geostatistical models to identify spatial distribution of groundwater quality parameters. *Environmental Science and Pollution Research* 29, 36512–36532. https://doi.org/10.1007/S11356-022-18639-8/TABLES/9

Fassoni-Andrade, A.C., Paiva, R.C.D. de, 2019. Mapping spatial-temporal sediment dynamics of river-floodplains in the Amazon. *Remote Sens. Environ.* 221, 94–107. https://doi.org/10.1016/J.RSE.2018.10.038

Fu, Q., Moerbeek, M., Hoijtink, H., 2022. Sample size determination for Bayesian ANOVAs with informative hypotheses. *Front. Psychol.* 13, 947768. https://doi.org/10.3389/FPSYG.2022.947768/BIBTEX

Gao, S., Dong, G., Jiang, X., Nie, T., Guo, X., 2023. Analysis of factors influencing spatiotemporal differentiation of the NDVI in the upper and middle reaches of the Yellow River from 2000 to 2020. *Front. Environ. Sci.* 10, 1072430. https://doi.org/10.3389/FENVS.2022.1072430

Gardner, J.R., Yang, X., Topp, S.N., Ross, M.R.V., Altenau, E.H., Pavelsky, T.M., 2021. The Color of Rivers. *Geophys Res. Lett.* 48, e2020GL088946. https://doi.org/10.1029/2020GL088946

Gensac, E., Martinez, J.M., Vantrepotte, V., Anthony, E.J., 2016. Seasonal and inter-annual dynamics of suspended sediment at the mouth of the Amazon river: The role of continental and oceanic forcing, and implications for coastal geomorphology and mud bank formation. *Cont. Shelf Res.* 118, 49–62. https://doi.org/10.1016/J.CSR.2016.02.009

Guillaume, M., Minghelli, A., Chami, M., Lei, M., 2023. Determination of Bayesian Cramér–Rao Bounds for Estimating Uncertainties in the Bio-Optical Properties of the Water Column, the Seabed Depth and Composition in a Coastal Environment. *Remote Sensing* 2023, Vol. 15, Page 2242 15, 2242. https://doi.org/10.3390/RS15092242

Guo, D., Lintern, A., Webb, J.A., Ryu, D., Liu, S., Bende-Michl, U., Leahy, P., Wilson, P., Western, A.W., 2019. Key Factors Affecting Temporal Variability in Stream Water Quality. *Water Resour. Res.* 55, 112–129. https://doi.org/10.1029/2018WR023370

Kupssinskü, L.S., Guimarães, T.T., De Souza, E.M., Zanotta, D.C., Veronez, M.R., Gonzaga, L., Mauad, F.F., 2020. A Method for Chlorophyll-a and Suspended Solids Prediction through Remote Sensing and Machine Learning. *Sensors* 2020, Vol. 20, Page 2125 20, 2125. https://doi.org/10.3390/S20072125

Moran, P.A.P., 1950. Notes on Continuous Stochastic Phenomena. Biometrika 37, 17. https://doi.org/10.2307/2332142

Morera, S.B., Condom, T., Crave, A., Steer, P., Guyot, J.L., 2017. The impact of extreme El Niño events on modern sediment transport along the western Peruvian Andes (1968–2012). *Scientific Reports* 2017 7:1 7, 1–14. https://doi.org/10.1038/s41598-017-12220-x

Pan, Y., Gong, J., Li, J., 2022. Assessment of Remote Sensing Ecological Quality by Introducing Water and Air Quality Indicators: A Case Study of Wuhan, China. *Land* 2022, Vol. 11, Page 2272 11, 2272. https://doi.org/10.3390/LAND11122272

Prestes, Y.O., Silva, A.C., Rollnic, M., Rosário, R.P., 2017. The M2 And M4 Tides in the Pará River Estuary. *Tropical Oceanography* 45, 26–37. https://doi.org/10.5914/TROPOCEAN.V45I1.15198

Prestes, Y.O., Borba, T.A. da C., Silva, A.C. da, Rollnic, M., 2020. A discharge stationary model for the Pará-Amazon estuarine system. *J. Hydrol. Reg. Stud.* 28, 100668. https://doi.org/10.1016/j.ejrh.2020.100668

Qiang, S., Song, K., Shang, Y., Lai, F., Wen, Z., Liu, G., Tao, H., Lyu, Y., 2023. Remote Sensing Estimation of CDOM and DOC with the Environmental Implications for Lake Khanka. *Remote Sens.* (Basel) 15, 5707. https://doi.org/10.3390/RS15245707/S1

Rosenberg, M.S., Anderson, C.D., 2011. PASSaGE: Pattern Analysis, Spatial Statistics and Geographic Exegesis. Version 2. Methods Ecol. Evol. 2, 229–232. https://doi.org/10.1111/J.2041-210X.2010.00081.X

Silva, L.G. da, Silva, G.E. de L. da, Silva, A.B. da, Menezes, R. de S., 2020. Modelagem da dinâmica evolutiva da qualidade da água na Baía do Guajará - Belém-PA/ Modeling of the evolutionary dynamics of water quality in Guajará Bay - Belém-PA. *Brazilian Journal of Development* 6, 4649–4660. https://doi.org/10.34117/BJDV6N1-333

SNAP Development Team, 2022. Geographic Resources Analysis Support System (GRASS) Software, Version 9.0.0. Open-Source European Space Agency. step.esa.int/main/download/snap-download (15 June 2022).

Toniolo, G.R., Guasselli, L.A., De Arruda, D.C., Pereira Filho, W., 2018. Identificação de constituintes opticamente ativos na água do Lago Guaíba a partir de dados de sensores orbitais e espectrorradiometria de campo. *Pesquisas em Geociências* 45, e0635–e0635. https://doi.org/10.22456/1807-9806.88645

Zhan, W., Wu, J., Wei, X., Tang, S., Zhan, H., 2019. Spatio-temporal variation of the suspended sediment concentration in

the Pearl River Estuary observed by MODIS during 2003–2015. *Cont Shelf Res* 172, 22–32. https://doi.org/10.1016/J.CSR.2018.11.007

Zhang, H., Yan, D., Zhang, B., Fu, Z., Li, B., Zhang, S., 2022. An Operational Atmospheric Correction Framework for Multi-Source Medium-High-Resolution Remote Sensing Data of China. *Remote Sensing* 2022, Vol. 14, Page 5590 14, 5590. https://doi.org/10.3390/RS14215590

Zhang, Y., Giardino, C., Li, L., 2017. Water Optics and Water color Remote Sensing. *Remote Sensing* 2017, Vol. 9, Page 818 9, 818. https://doi.org/10.3390/RS9080818